

Fast Scrambling in Hyperbolic Ising Model

Goksu Can Toga,^{1,*} Abhishek Samlodia,^{2,†} and Alexander F. Kemper^{1,‡}

¹*Department of Physics, North Carolina State University, Raleigh, NC 27695, USA*

²*Department of Physics, Syracuse University, Syracuse, NY 13244, USA*

(Dated: March 4, 2025)

We investigate many-body chaos and scrambling in the Hyperbolic Ising model, a mixed-field Ising model living in the background of AdS_2 . The effect of the curvature is captured by site-dependent couplings obtained from the AdS_2 metric applied to a flat nearest neighbor spin chain. We show that this model with only local site-dependent nearest neighbor interactions is maximally chaotic, can be classified as a fast scrambler, and saturates the Maldacena-Shenker-Stanford (MSS) bound on chaos for a certain set of parameters, thus making this model one of the few if not the only example where such fast scrambling behavior has been seen without all-to-all or long-range interactions. Moreover, the modest resources needed to simulate this model make it an ideal test-bed for studying scrambling and chaos on quantum computers.

PACS numbers:

I. INTRODUCTION

Quantum many-body chaos and scrambling have attracted a great deal of attention in recent years, from more theoretical endeavors like studying the scrambling dynamics of black holes using their dual descriptions [1–7] to more practical applications like investigating scrambling in chemical reactions to quantum cryptography [8, 9] and many more.

In almost all of these studies, the Sachdev-Ye-Kitaev (SYK) model has been the center of attention as the quintessential example of a model that exhibits fast scrambling and quantum chaos [10–13]. However, due to the all-to-all and random interactions in this model, any kind of classical and quantum simulation can be very challenging and often requires various truncations and approximations [14–17]. In this letter, we advocate for a new model that is also maximally chaotic and exhibits fast scrambling but with only local site-dependent interactions.¹

A wide variety of tests have been developed to diagnose and classify quantum chaos, including spectral form factors [24–26], level statistics [27, 28], different definitions of complexity [29, 30], Loschmidt echos [31–33] and out-of-time ordered correlators (OTOCs) [34, 35]. Out of these many tools, Krylov Complexity — which can be defined for both states and operators — and OTOCs have emerged as the most comprehensive tests and have become the primary norm for diagnosing quantum chaos in many body systems [36–46].

While OTOCs have become the leading test in clas-

sifying quantum chaos and scrambling, their calculation is cumbersome and the numerical analysis of extracting Lyapunov exponents from OTOCs requires carefully fitting an exponential in a narrow parameter window. On the other hand, we have diagnostic tools that are based on Krylov subspace methods which do not require a fitting process as delicate as the OTOCs; however, due to the numerical instabilities in the Lanczos algorithm they require either a full or partial re-orthogonalization procedures limiting the system sizes that can be reached with these methods [47]. Here, we use both of these techniques to give a complete picture that encompasses large system sizes and a concrete diagnostic of quantum chaos and scrambling.

A summary of our results can be seen in Fig. 1, where a simple model inspired by holography — the Hyperbolic Ising model — satisfies multiple criteria of quantum chaos and fast scrambling. We evaluate the scrambling time t_s and find a logarithmic lightcone, with $t_s \sim \log(N)$, where N is the number of spins. The Lyapunov exponents obtained from OTOCs at finite temperatures decay as a/β , where $\beta = 1/T$ is the inverse temperature and a is a constant. Most importantly, the decay of these Lyapunov exponents for a certain set of parameters saturates the Maldacena-Shenker-Stanford (MSS) bound on chaos [35]. We also study the Krylov state complexity (K-complexity), which exhibits the expected ramp-peak-plateau behavior [41, 42], the Krylov Entropy (K-entropy) which rises exponentially at early times, and the Krylov operator complexity which shows the expected exponential-linear-saturation behavior [36–38]; all of these are indicative of fast scrambling and chaos.

These tests provide strong evidence that this model exhibits quantum chaos and can be classified as a fast scrambler, giving us one of the few examples where a fast scrambling behavior has been seen outside of the SYK model and the only example with computational resources needed for its classical and quantum simulations similar to the mixed field Ising model. This dis-

*Electronic address: gctoga@ncsu.edu

†Electronic address: asamlodi@syr.edu

‡Electronic address: akemper@ncsu.edu

¹ There are other examples of fast scrambling models besides the SYK model but to the best of our knowledge they all require longer-range interactions than nearest neighbor interactions to be present in the model [18–23].

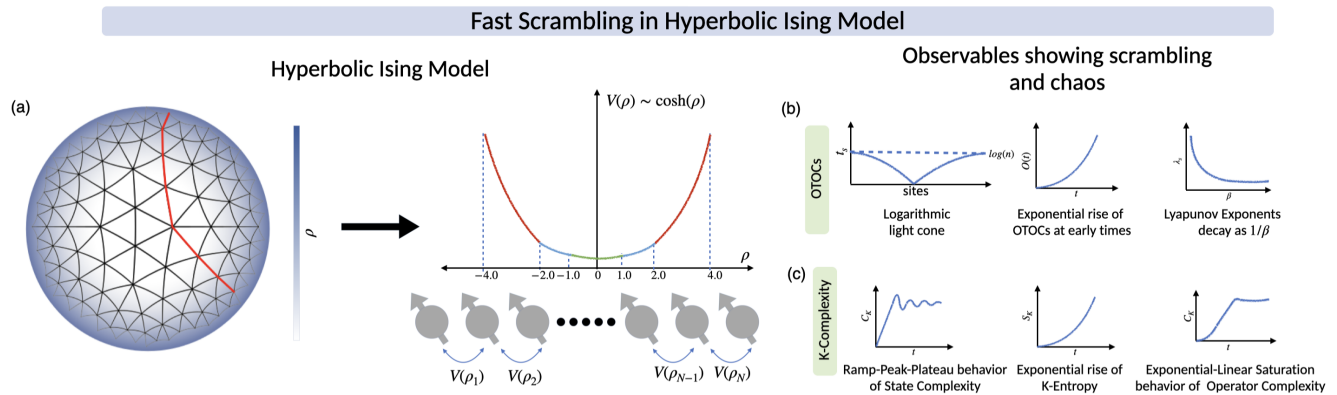


FIG. 1: a) Left: Tesselation of the Poincaré disk. The red line displays the line we choose to obtain the AdS_2 Ising model; the spins are located at the vertices. Right: Site-dependent nearest neighbor couplings applied to a flat spin chain to capture the curved background. Different colors on the line plot show how our site-dependent coupling changes according to different l_{\max} values. b,c) Checks for scrambling and chaos in the hyperbolic Ising model, (b) using tensor networks for OTOCs, and (c) using Krylov subspace methods.

covery opens new avenues of research where we can use locally varying interactions to control different behaviors of scrambling and information propagation in quantum systems and test quantum chaos and scrambling without incurring the potentially heavy computational costs of an all-to-all connected model.

II. HYPERBOLIC ISING MODEL

Our model of interest, the Hyperbolic Ising model is a mixed field Ising (MFI) model formulated on a one-dimensional hyperbolic space. In Fig. 1 we show how one can visualize this model as a line between two boundary points in AdS_3 and interpret the effects of the background curvature as site-dependent couplings.

The Hamiltonian that describes this Ising chain can be given as [48–52],

$$\begin{aligned} \hat{H} = & -J \sum_i \left(\frac{\eta_i + \eta_{i+1}}{2} \right) \sigma_i^z \sigma_{i+1}^z \\ & + h \sum_i \eta_i \sigma_i^x + m \sum_i \eta_i \sigma_i^z, \end{aligned} \quad (1)$$

with $\eta_i = \cosh(\rho_i)$

where σ_i^p is a local Pauli operator at site i with $p \in \{x, y, z\}$. The local site-dependent coupling terms for the Ising chain, $\eta_i = \cosh(\rho_i) \sim \sqrt{g}$ arise from the Euclidean metric of AdS_2 ,

$$ds^2 = \ell^2 (\cosh^2(\rho) dt^2 + d\rho^2) \quad (2)$$

To obtain the couplings in Eq. 1 we set $\ell = 1.0$ and discretize radius of curvature ρ as follows,

$$\rho_i = -l_{\max} + i \frac{2l_{\max}}{N-1} \quad (3)$$

here N is the size of the spin chain and l_{\max} controls the curvature of the underlying curved space. One can easily recover the flat mixed field Ising model by taking the $l_{\max} \rightarrow 0$ limit. This model exhibits a phase transition at $J/h = 1.0$ for a small value of the parameter m similar to the flat Ising model [48].

In the rest of the paper, we will center our discussion around this critical point where the mixed field Ising model is known to be chaotic [53] and show that the inclusion of the curved background enhances this chaotic behavior and introduces fast scrambling.

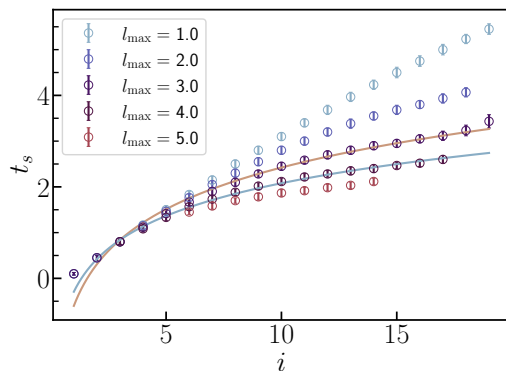


FIG. 2: Scrambling time t_s as a function of site index i for $N = 37$, $l_{\max} = (1.0, \dots, 5.0)$ at infinite temperature showing the lightcone changing from linear to logarithmic as a function of l_{\max} .

In an earlier work [48], we investigated information propagation and scrambling in this model in the infinite temperature limit, and showed that for a suitable subset of the parameters the lightcone obtained from infinite temperature OTOCs is logarithmic such that the saturation time $t_s \sim \log(i)$ where i is the site index which

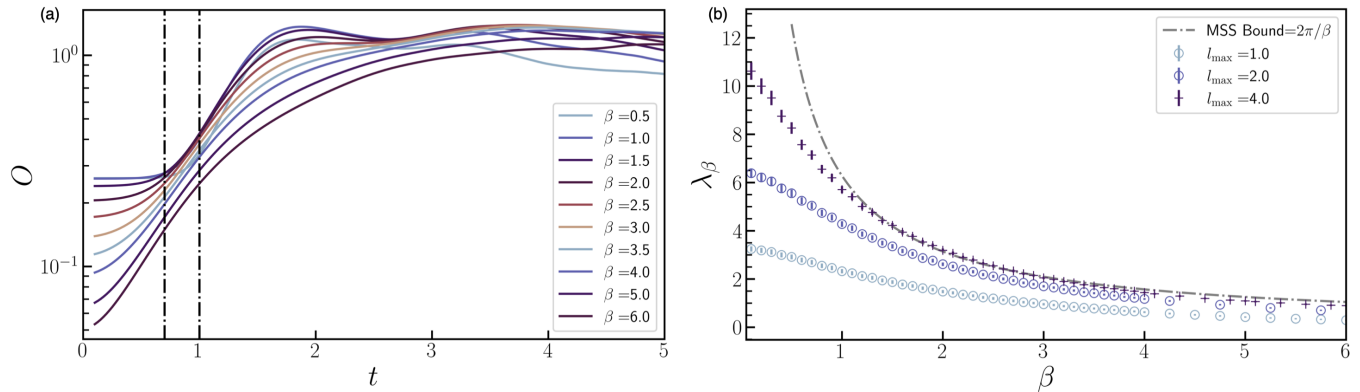


FIG. 3: a) O for $N = 13$, $J/h = 1.0$, $m = 0.05$, and $l_{\max} = 4.0$ black dashed lines show the fitting range we used in extracting the Lyapunov exponents. b) The Lyapunov exponent λ_β ; for $l_{\max} = (1.0, 2.0, 4.0)$. Notice that λ_β starts saturating the MSS bound as the background curvature is increased. Error bounds are obtained from the confidence intervals of the fitting.

implies that $t_s \sim \log(N)$ for a system of N spins. This logarithmic spreading can be seen in Fig. 2 where lines show fits to a logarithmic function, and it is one of the tell-tale signs of fast scrambling [34]. Surprisingly, this simple model with local interactions captures this behavior quite easily due to its unique site-dependent couplings arising from the curved background contrary to the usual expectations that require all-to-all or long-range interactions to achieve such behavior.

III. OBSERVABLES FOR CHAOS AND FAST SCRAMBLING

Motivated by the observations of logarithmic lightcones in this model, we will provide further evidence that this model is indeed chaotic and can be classified as a fast-scrambler by investigating finite temperature OTOCs and various complexity measures defined using Krylov subspace methods.

A. OTOCs at Finite Temperature

OTOCs are one of the most heavily used diagnostic tools for scrambling and chaos. They are obtained from the double commutator of operators $W(t) = e^{iHt}W e^{-iHt}$ and V and can be given as follows.

$$F_{ij}(t) = \frac{1}{Z} \text{Tr} [e^{-\beta H} W_i(t) V_j W_i(t) V_j] \quad (4)$$

where $Z = \text{Tr}(e^{-\beta H})$ and $\beta = 1/T$.

For a chaotic system, OTOCs are expected to decay as $F_\beta(t) \sim e^{-\lambda_\beta t}$ for times before scrambling time, where λ_β is the Lyapunov exponent and can be thought of as the quantum counterpart of the classical Lyapunov exponent.

For systems at finite temperatures, it is common to employ a regularized definition for the OTOCs due to

divergences [35]. This regularized form for the OTOCs can be defined as

$$\tilde{F}_{ij}(t) = \text{Tr} [\alpha W_i(t) \alpha V_j \alpha W_i(t) \alpha V_j], \quad (5)$$

where $\alpha^4 = Z^{-1} e^{-\beta H}$.

As discussed earlier, we will choose $J/h = 1.0$, and $m = 0.05$ such that the model is near the chaotic region of the mixed field Ising model and choose W_i , and V_j as $\sigma_{\frac{N+1}{2}}^z$ and σ_1^z respectively and obtain the finite temperature states that go into this calculation by purification techniques [54, 55] developed for Matrix Product States (MPS)² [57–62].

After the desired thermal state is obtained it is then time evolved while measuring $O = 1 - \tilde{F}_{ij}(t)$ at each time-step. In Fig. 3 we show our results for the OTOCs at $l_{\max} = 4.0$ at inverse temperatures ranging from $\beta = [0.5, \dots, 6.0]$. To extract the Lyapunov exponents we fit $\log(\frac{dO}{dt})$ to $f(x) = at + b$; this approach yields better fits with better R^2 results compared to exponential fits of the original function.

Our results presented in Fig. 3 (a) confirm the expected exponential rise of the OTOCs with the two dashed lines indicating the fitting range. This range is chosen such that for all the values of β the linear fits result in a $R^2 \geq 0.96$.

Fig. 3 (b) shows the decay of the λ_β as a/β where a is some constant. Most importantly we clearly see that as the background curvature is increased the Lyapunov exponents start saturating the Maldacena-Shenker-Stanford (MSS) bound on chaos which is the most famous criterion for fast scrambling.

Although our results show agreement with the MSS bound we note that this result is highly dependent on

² For tensor network simulations we used the ITensor Library [56]; details of our simulation procedure can be found in Appendix. B.

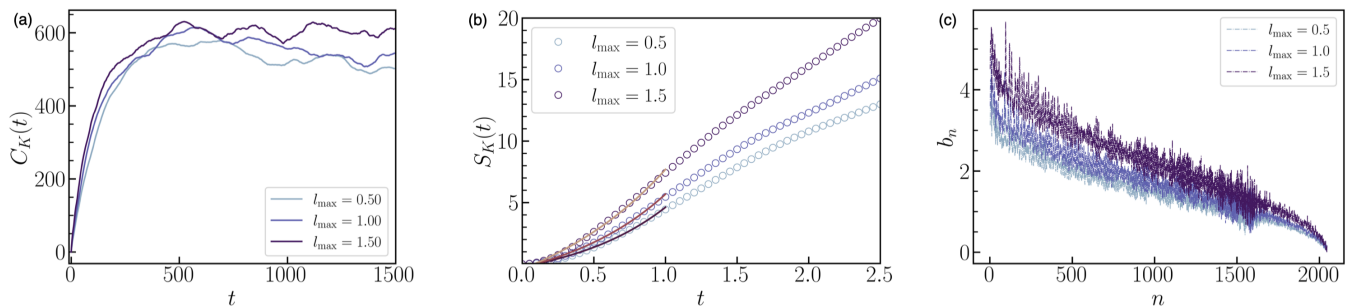


FIG. 4: a) C_K using states for $N = 11$, $J/h = 1.0$, $m = 0.05$ at different l_{\max} values showing the ramp-peak-plateau behavior. b) S_K for the same set of parameters showing the expected exponential behavior. c) Lanczos coefficients as a function of the state index n which shows the expected linear dependence on n .

choosing the right fitting window. The dependence of $1/\beta$ is less sensitive in changes to this window but the coefficient of the fit is and thus can affect the temperature range where the MSS bound is satisfied. We also note that due to the Trotterized evolution used in both obtaining the thermal state and the time-evolved states, we are limited to moderate values of β that can be simulated reliably due to the accumulation of Trotter errors.

Nevertheless, combining the $1/\beta$ decay of the Lyapunov exponents with the fact that we get a logarithmic lightcone for the same sets of parameters provides compelling evidence of fast scrambling.

B. Krylov Observables

Now we switch gears and discuss our observables obtained using Krylov subspace methods. The main advantage of these observables is that they do not require a delicate fitting scheme like OTOCs do to diagnose chaos.

The two quantities of interest are the state and operator version of the K-complexity C_K and Krylov Entropy $S_K(t)$ calculated using states. These observables obtained from the Krylov basis wavefunctions exhibit different characteristics for integrable and chaotic systems allowing them to be used as a diagnostic tool for quantum chaos [36–41]. The Krylov complexity $C_K(t)$ and Krylov Entropy $S_K(t)$ for states can be defined as,

$$C_K(t) = \sum_{n=0}^{\mathbb{K}-1} n |\phi_n(t)|^2 \quad (6)$$

$$S_K(t) = - \sum_{n=0}^{\mathbb{K}-1} |\phi_n(t)|^2 \ln (|\phi_n(t)|^2) \quad (7)$$

where $\phi_n(t)$ are the Krylov basis wavefunctions obtained via Lanczos algorithm [63] with $\mathbb{K} = \dim(K)$, is the dimension of the Krylov subspace K .

The dynamics in the Krylov subspace are fully determined by the time evolution of Krylov wavefunctions and due to the tridiagonal structure of the Lanczos coeffi-

cients time evolution in the Krylov subspace simplifies to the following recursion relation [47].

$$\dot{\phi}_n(t) = b_n \phi_{n-1}(t) - b_{n+1} \phi_{n+1}(t) \quad (8)$$

Here $\{(a_n, b_n)\}_{n=0}^{\mathbb{K}-1}$ are the Lanczos coefficients obtained via the Lanczos algorithm [63] and the equations can be solved with the initial condition $\phi_n(t=0) = \delta_{n0}$.

Furthermore, these recursion relations map the time evolution in the full space to a single particle hopping model in the one-dimensional Krylov chain making long-time simulations tractable, especially for time scales where our tensor network methods break down. More details about the Lanczos algorithm and our implementation can be found in the Appendix. A

This brings us to our first set of observables that signals a chaotic system in the context of Krylov methods. We start the Lanczos algorithm with the state $\bigotimes_{i=1}^N |+\rangle^y$, where $|+\rangle^y = \frac{1}{\sqrt{2}} (|0\rangle^y + i |1\rangle^y)$. We chose this initial seed choice because in the flat Ising model this state exhibited a clear peak in $C_K(t)$ in the chaotic regime of the model [42].³ Using this initial choice we carry out the subspace generation and time evolution and investigate $C_K(t)$ and $S_K(t)$.

There are three key indicators of quantum chaos obtained using states. First, $C_K(t)$ is expected to exhibit ramp-peak-plateau behavior in time. Next, $S_K(t)$ should exhibit an exponential behavior at early timescales. Finally, the Lanczos coefficients b_n should have a linear relationship with n , where $0 \leq n \leq \mathbb{K} - 1$ [36–41].

Our results confirm the expectations described above and show the system becomes more chaotic as the background curvature increases. In Fig. 4 (a) we show the $C_K(t)$ where the ramp-peak-plateau behavior is clearly

³ The choice of the initial seed is an essential part of this algorithm and it can have an effect on the results obtained for $C_K(t)$ and $S_K(t)$. To alleviate this dependence on the initial seed new algorithms that sample a wide array of initial seeds have been proposed [64].

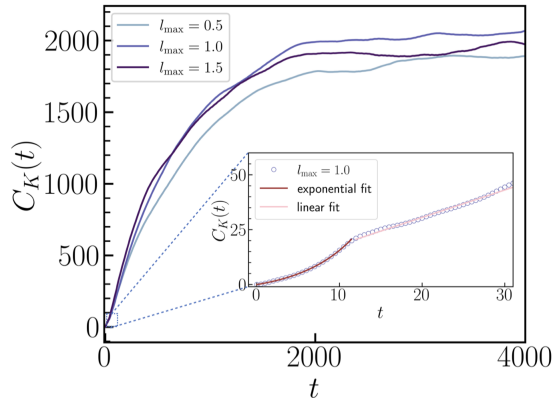


FIG. 5: Operator Complexity for $N = 6, J/h = 1.0, m = 0.05$. Inset shows the change from exponential to linear behavior around the scrambling times.

visible and the peak becomes more prominent as we increase l_{\max} in line with the expectation that the model becomes more chaotic as l_{\max} is increased. In Fig. 4 (b) we show $S_K(t)$ which shows the expected exponential rise, the lines show fits to a function of form $f(t) = a(e^c - d)$ and the factor c increases with l_{\max} . Finally, in Fig. 4 (c), we show the Lanczos coefficient b_n vs n which shows the linear dependence on n , providing us with three more tests signaling chaos.

The next set of observables are based on calculations using operators instead of states. Lanczos algorithm can be generalized to operators in straightforward way using the channel-state duality [65]. In this case, the Hamiltonian becomes a Liouvillian that acts on the operators, and the usual inner product $\langle p|q \rangle$ of quantum states in Lanczos Algorithm is changed to $\langle A|B \rangle := \frac{1}{D} \text{Tr} [A^\dagger B]$. We choose σ_1^z as our initial seed operator for the Lanczos algorithm and carry out the subspace generation and time-evolution.

The $C_K(t)$ obtained using the operators is closely related to operator growth in the full model and hence can be used to identify scrambling behavior and chaos [38]. For a fast scrambler, operator complexity is expected to grow exponentially at early timescales followed by a linear increase and finally, they saturate/oscillate about some fixed average value related to the dimension of the Krylov subspace [66].

Fig. 5 confirms this expected behavior for a chaotic system with the inset showing the early time dynamics of the complexity which is fitted to an exponential followed by a linear function. Confirming our discovery of scrambling in the Hyperbolic Ising model.

IV. CONCLUSIONS AND OUTLOOK

In this paper, we investigated chaos and scrambling in the Hyperbolic Ising model which is a nearest neighbor mixed field Ising model with site-dependent couplings

using tensor network and Krylov subspace methods and showed that the observables obtained from both of these independent techniques show signatures of fast scrambling and chaos. More specifically we had three main observables with such a signature.

Using tensor networks we showed that, for a suitable subset of the parameter space we observed a logarithmic lightcone with scrambling time $t_s \sim \log(N)$. Finite temperature OTOCs showed the expected exponential rise at early times similar to the operator complexity, with Lyapunov exponents obtained from these exponentials decaying as a/β while saturating the MSS bound for a certain set of parameters.

With the Krylov subspace methods, we showed that the observables obtained using states exhibit the following signatures of chaos. K-Complexity demonstrated the expected ramp-peak-plateau behavior with the peak scaling according to the background curvature l_{\max} . Next, K-Entropy showed the expected exponential rise at early times. Finally, we showed that Lanczos coefficients b_n depend linearly on n which is another criterion of chaos.

Operator complexity showed an exponential rise similar to the OTOCs at early times followed by a linear increase, and saturation around a maximum at late times.

Combining these results, we see robust evidence that this model can be classified as a fast scrambler. This provides us with a unique model in the class of fast scramblers where with only nearest-neighbor interactions and site-dependent couplings fast scrambling behavior can be achieved. In addition, in Fig. 2 we showed that it is possible to switch between different scrambling behaviors with ease in this model ranging from the slowest linear spreading to the fastest logarithmic spreading and anything in between by adjusting the background curvature and nearest neighbor coupling J .

This opens up new possibilities for studying scrambling and chaos on classical and quantum computers in detail, where we now have access to a model where by changing just two parameters we can have complete control of different kinds of scrambling behavior with modest requirements needed for its simulations compared to all-to-all connected models making it easily accessible for future studies.

In addition to the fast scrambling behavior, simulations of models that exhibit AdS/CFT correspondence are interesting in and of themselves due to the close connection between holographic models and error correcting codes [67–71]; having an efficient way of simulating these models on quantum computers could benefit the study of such codes.

Acknowledgments

We thank Raghav Govind Jha and Bharath Sambasivam for valuable discussions. AFK and GCT acknowledge financial support from the National Science Foundation under award No. 2325080: PIF: Software-Tailored

Architecture for Quantum Co-Design. AS is supported by U.S. Department of Energy grant DE-SC0019139. We acknowledge the computing resources provided by North

Carolina State University High Performance Computing Services Core Facility (RRID:SCR_022168).

-
- [1] B. Kobrin, Z. Yang, G. D. Kahanamoku-Meyer, C. T. Olund, J. E. Moore, D. Stanford, and N. Y. Yao, *Physical Review Letters* **126**, 030602 (2021), ISSN 0031-9007, 1079-7114, URL <https://link.aps.org/doi/10.1103/PhysRevLett.126.030602>.
- [2] W. Fu and S. Sachdev, *Phys. Rev. B* **94**, 035135 (2016), URL <https://link.aps.org/doi/10.1103/PhysRevB.94.035135>.
- [3] M. Asaduzzaman, R. G. Jha, and B. Sambasivam, *Physical Review D* **109**, 105002 (2024), ISSN 2470-0010, 2470-0029, arXiv:2311.17991 [quant-ph], URL <http://arxiv.org/abs/2311.17991>.
- [4] A. R. Brown, H. Gharibyan, S. Leichenauer, H. W. Lin, S. Nezami, G. Salton, L. Susskind, B. Swingle, and M. Walter, *PRX Quantum* **4**, 010320 (2023), ISSN 2691-3399, arXiv:1911.06314 [hep-th, physics:quant-ph], URL <http://arxiv.org/abs/1911.06314>.
- [5] T. Schuster, B. Kobrin, P. Gao, I. Cong, E. T. Khabiboulline, N. M. Linke, M. D. Lukin, C. Monroe, B. Yoshida, and N. Y. Yao, *Physical Review X* **12**, 031013 (2022), ISSN 2160-3308, URL <https://link.aps.org/doi/10.1103/PhysRevX.12.031013>.
- [6] J. S. Cotler, G. Gur-Ari, M. Hanada, J. Polchinski, P. Saad, S. H. Shenker, D. Stanford, A. Streicher, and M. Tezuka, *Journal of High Energy Physics* **2017**, 118 (2017), ISSN 1029-8479, arXiv:1611.04650 [hep-th], URL <http://arxiv.org/abs/1611.04650>.
- [7] L. K. Joshi, A. Elben, A. Vikram, B. Vermersch, V. Galitski, and P. Zoller, *Physical Review X* **12**, 011018 (2022), ISSN 2160-3308, arXiv:2106.15530 [cond-mat, physics:hep-th, physics:nlin, physics:quant-ph], URL <http://arxiv.org/abs/2106.15530>.
- [8] C. Chamon, E. R. Mucciolo, A. E. Ruckenstein, and Z.-C. Yang, *npj Quantum Information* **10**, 37 (2024).
- [9] C. Chamon, E. R. Mucciolo, and A. E. Ruckenstein, *Annals of Physics* **446**, 169086 (2022).
- [10] S. Sachdev and J. Ye, *Phys. Rev. Lett.* **70**, 3339 (1993), URL <https://link.aps.org/doi/10.1103/PhysRevLett.70.3339>.
- [11] *Alexei Kitaev, Caltech & KITP, A simple model of quantum holography (part 1)*, URL <https://online.kitp.ucsb.edu/online/entangled15/kitaev/>.
- [12] *Alexei Kitaev, Caltech, A simple model of quantum holography (part 2)*, URL <https://online.kitp.ucsb.edu/online/entangled15/kitaev2/>.
- [13] J. Maldacena and D. Stanford, *Physical Review D* **94**, 106002 (2016), ISSN 2470-0010, 2470-0029, URL <https://link.aps.org/doi/10.1103/PhysRevD.94.106002>.
- [14] S. Xu, L. Susskind, Y. Su, and B. Swingle, *A Sparse Model of Quantum Holography* (2020), arXiv:2008.02303 [cond-mat], URL <http://arxiv.org/abs/2008.02303>.
- [15] A. M. García-García, Y. Jia, D. Rosa, and J. J. Verbaarschot, *Physical Review D* **103**, 106002 (2021), ISSN 2470-0010, 2470-0029, URL <https://link.aps.org/doi/10.1103/PhysRevD.103.106002>.
- [16] Y. Cao, Y.-N. Zhou, T.-T. Shi, and W. Zhang, *Science Bulletin* **65**, 1170 (2020), ISSN 2095-9273, URL <https://www.sciencedirect.com/science/article/pii/S2095927320301808>.
- [17] C. Sünderhauf, L. Piroli, X.-L. Qi, N. Schuch, and J. I. Cirac, *Journal of High Energy Physics* **2019**, 38 (2019), ISSN 1029-8479, URL [https://doi.org/10.1007/JHEP11\(2019\)038](https://doi.org/10.1007/JHEP11(2019)038).
- [18] T. Hashizume, G. S. Bentsen, S. Weber, and A. J. Daley, *Phys. Rev. Lett.* **126**, 200603 (2021), URL <https://link.aps.org/doi/10.1103/PhysRevLett.126.200603>.
- [19] Z. Li, S. Choudhury, and W. V. Liu, *Phys. Rev. Res.* **2**, 043399 (2020), URL <https://link.aps.org/doi/10.1103/PhysRevResearch.2.043399>.
- [20] N. Lashkari, D. Stanford, M. Hastings, T. Osborne, and P. Hayden, *Journal of High Energy Physics* **2013**, 22 (2013), ISSN 1029-8479, arXiv:1111.6580 [hep-th, physics:quant-ph], URL <http://arxiv.org/abs/1111.6580>.
- [21] R. Belyansky, P. Bienias, Y. A. Kharkov, A. V. Gorshkov, and B. Swingle, *Phys. Rev. Lett.* **125**, 130601 (2020), URL <https://link.aps.org/doi/10.1103/PhysRevLett.125.130601>.
- [22] C. Yin and A. Lucas, *Phys. Rev. A* **102**, 022402 (2020), URL <https://link.aps.org/doi/10.1103/PhysRevA.102.022402>.
- [23] G. Bentsen, Y. Gu, and A. Lucas, *Proceedings of the National Academy of Sciences* **116**, 6689 (2019).
- [24] P. Kos, M. Ljubotina, and T. c. v. Prosen, *Phys. Rev. X* **8**, 021062 (2018), URL <https://link.aps.org/doi/10.1103/PhysRevX.8.021062>.
- [25] J. Liu, *Phys. Rev. D* **98**, 086026 (2018), URL <https://link.aps.org/doi/10.1103/PhysRevD.98.086026>.
- [26] B. Bertini, P. Kos, and T. c. v. Prosen, *Phys. Rev. Lett.* **121**, 264101 (2018), URL <https://link.aps.org/doi/10.1103/PhysRevLett.121.264101>.
- [27] M. V. Berry and M. Tabor, *Proceedings of the Royal Society of London. A. Mathematical and Physical Sciences* **356**, 375 (1977).
- [28] O. Bohigas, M.-J. Giannoni, and C. Schmit, *Physical review letters* **52**, 1 (1984).
- [29] D. A. Roberts and B. Yoshida, *Journal of High Energy Physics* **2017**, 1 (2017).
- [30] V. Balasubramanian, P. Caputa, J. M. Magan, and Q. Wu, *Physical Review D* **106**, 046007 (2022).
- [31] A. Peres, *Physical Review A* **30**, 1610 (1984).
- [32] R. A. Jalabert and H. M. Pastawski, *Physical review letters* **86**, 2490 (2001).
- [33] T. Gorin, T. Prosen, T. H. Seligman, and M. Žnidarič, *Physics Reports* **435**, 33 (2006).
- [34] Y. Sekino and L. Susskind, *Journal of High Energy Physics* **2008**, 065 (2008), ISSN 1029-8479, arXiv:0808.2096 [hep-th, physics:quant-ph], URL <http://arxiv.org/abs/0808.2096>.
- [35] J. Maldacena, S. H. Shenker, and D. Stanford, *JHEP* **08**, 106 (2016), 1503.01409.
- [36] D. E. Parker, X. Cao, A. Avdoshkin, T. Scaffidi,

- and E. Altman, *A Universal Operator Growth Hypothesis* (2019), arXiv:1812.08657 [cond-mat, physics:hep-th, physics:nlin, physics:quant-ph], URL <http://arxiv.org/abs/1812.08657>.
- [37] E. Rabinovici, A. Sánchez-Garrido, R. Shir, and J. Sonner, *Journal of High Energy Physics* **2022**, 151 (2022), ISSN 1029-8479, arXiv:2207.07701 [cond-mat, physics:hep-th, physics:quant-ph], URL <http://arxiv.org/abs/2207.07701>.
- [38] P. Nandy, A. S. Matsoukas-Roubeas, P. Martínez-Azcona, A. Dymarsky, and A. del Campo, *Quantum Dynamics in Krylov Space: Methods and Applications* (2024), arXiv:2405.09628 [cond-mat, physics:hep-th, physics:nlin, physics:quant-ph], URL <http://arxiv.org/abs/2405.09628>.
- [39] M. Baggioli, K.-B. Huh, H.-S. Jeong, K.-Y. Kim, and J. F. Pedraza, *Krylov complexity as an order parameter for quantum chaotic-integrable transitions* (2024), arXiv:2407.17054 [hep-th, physics:nlin, physics:quant-ph], URL <http://arxiv.org/abs/2407.17054>.
- [40] S. Chapman, S. Demulder, D. A. Galante, S. U. Sheorey, and O. Shoval, *Krylov complexity and chaos in deformed SYK models* (2024), arXiv:2407.09604 [cond-mat, physics:hep-th, physics:quant-ph], URL <http://arxiv.org/abs/2407.09604>.
- [41] R. G. Jha and R. Roy (2024), 2407.20569.
- [42] M. Alishahiha, S. Banerjee, and M. J. Vasli, *Krylov Complexity as a Probe for Chaos* (2024), arXiv:2408.10194 [hep-th, physics:quant-ph], URL <http://arxiv.org/abs/2408.10194>.
- [43] B. Swingle, *Nature Phys.* **14**, 988 (2018).
- [44] C.-J. Lin and O. I. Motrunich, *Phys. Rev. B* **97**, 144304 (2018), URL <https://link.aps.org/doi/10.1103/PhysRevB.97.144304>.
- [45] I. García-Mata, R. A. Jalabert, and D. A. Wisniacki, *Scholarpedia* **18**, 55237 (2023), 2209.07965.
- [46] A. Schuckert and M. Knap, *SciPost Phys.* **7**, 022 (2019), URL <https://scipost.org/10.21468/SciPostPhys.7.2.022>.
- [47] A. Sánchez-Garrido, Ph.D. thesis, U. Geneva (main) (2024), 2407.03866.
- [48] M. Asaduzzaman, S. Catterall, Y. Meurice, and G. C. Toga, *Phys. Rev. D* **109**, 054513 (2024), URL <https://link.aps.org/doi/10.1103/PhysRevD.109.054513>.
- [49] H. Ueda, H. Nakano, K. Kusakabe, and T. Nishino, *Journal of the Physical Society of Japan* **80**, 094001 (2011), ISSN 0031-9015, 1347-4073, arXiv:1102.0845 [cond-mat], URL <http://arxiv.org/abs/1102.0845>.
- [50] H. Ueda, A. Gendiar, V. Zauner, T. Iharagi, and T. Nishino, *Transverse Field Ising Model Under Hyperbolic Deformation* (2010), arXiv:1008.3458 [cond-mat, physics:quant-ph], URL <http://arxiv.org/abs/1008.3458>.
- [51] H. Ueda, H. Nakano, K. Kusakabe, and T. Nishino, *Progress of Theoretical Physics* **124**, 389 (2010), ISSN 0033-068X, 1347-4081, arXiv:1006.2652 [cond-mat, physics:quant-ph], URL <http://arxiv.org/abs/1006.2652>.
- [52] R. C. Brower, C. V. Cofburn, and E. Owen, *Phys. Rev. D* **105**, 114503 (2022), 2202.03464.
- [53] M. C. Bañuls, J. I. Cirac, and M. B. Hastings, *Phys. Rev. Lett.* **106**, 050405 (2011), URL <https://link.aps.org/doi/10.1103/PhysRevLett.106.050405>.
- [54] A. E. Feiguin and S. R. White, *Phys. Rev. B* **72**, 220401 (2005), URL <https://link.aps.org/doi/10.1103/PhysRevB.72.220401>.
- [55] A. M. Alhambra and J. I. Cirac, *PRX Quantum* **2**, 040331 (2021), URL <https://link.aps.org/doi/10.1103/PRXQuantum.2.040331>.
- [56] M. Fishman, S. R. White, and E. M. Stoudenmire (2020), 2007.14822.
- [57] S. R. White and A. E. Feiguin, *Physical review letters* **93**, 076401 (2004).
- [58] S. R. White, *Phys. Rev. B* **48**, 10345 (1993), URL <https://link.aps.org/doi/10.1103/PhysRevB.48.10345>.
- [59] U. Schollwöck, *Rev. Mod. Phys.* **77**, 259 (2005), URL <https://link.aps.org/doi/10.1103/RevModPhys.77.259>.
- [60] G. Vidal, *Phys. Rev. Lett.* **91**, 147902 (2003), URL <https://link.aps.org/doi/10.1103/PhysRevLett.91.147902>.
- [61] F. Verstraete, J. J. Garcia-Ripoll, and J. I. Cirac, *Physical review letters* **93**, 207204 (2004).
- [62] G. Vidal, *Phys. Rev. Lett.* **93**, 040502 (2004), URL <https://link.aps.org/doi/10.1103/PhysRevLett.93.040502>.
- [63] C. Lanczos, *Journal of Research of the National Bureau of Standards* **45**, 255–282 (1950).
- [64] B. Craps, O. Evnin, and G. Pascuzzi, *Phys. Rev. Lett.* **134**, 050402 (2025), URL <https://link.aps.org/doi/10.1103/PhysRevLett.134.050402>.
- [65] M. Jiang, S. Luo, and S. Fu, *Phys. Rev. A* **87**, 022310 (2013), URL <https://link.aps.org/doi/10.1103/PhysRevA.87.022310>.
- [66] J. Barbón, E. Rabinovici, R. Shir, and R. Sinha, *Journal of High Energy Physics* **2019**, 264 (2019), ISSN 1029-8479, URL [https://doi.org/10.1007/JHEP10\(2019\)264](https://doi.org/10.1007/JHEP10(2019)264).
- [67] F. Pastawski, B. Yoshida, D. Harlow, and J. Preskill, *Journal of High Energy Physics* **2015**, 1 (2015).
- [68] C. Zhang, S. Kundu, N. Makri, M. Gruebele, and P. G. Wolynes, *Proceedings of the National Academy of Sciences* **121**, e2321668121 (2024), <https://www.pnas.org/doi/pdf/10.1073/pnas.2321668121>, URL <https://www.pnas.org/doi/abs/10.1073/pnas.2321668121>.
- [69] V. Chandrasekaran and A. Levine, *Journal of High Energy Physics* **2022**, 39 (2022), ISSN 1029-8479, arXiv:2203.05058 [cond-mat, physics:hep-th, physics:quant-ph], URL <http://arxiv.org/abs/2203.05058>.
- [70] W. Wang, *Building holographic code from the boundary* (2024), arXiv:2407.10271 [quant-ph], URL <http://arxiv.org/abs/2407.10271>.
- [71] A. Almheiri, X. Dong, and D. Harlow, *JHEP* **04**, 163 (2015), 1411.7041.

Appendix A: Krylov Subspace Methods

Krylov methods are one of the widely used numerical techniques for dealing with large matrices, particularly obtaining their characteristic equations. However, for quantum mechanical systems, such methods have proven to be useful in studying time evolution of quantum states/operators without exactly diagonalizing

the Hamiltonian for a system. The method is based on the Lanczos algorithm which can be summarized as follows [47, 63],

1. Set $|K_0\rangle = |v_0\rangle$, where $|v_0\rangle$ is the initial state you start with.
2. $a_0 = \langle K_0|H|K_0\rangle$
3. Loop over n , where $n \geq 1$
 - (a) $|A_n\rangle = H|K_{n-1}\rangle$
 - (b) FRO : $|A_n\rangle \rightarrow |A_n\rangle - \sum_{m=0}^{n-1} \langle K_m|A_n\rangle |K_m\rangle$
 - (c) $b_n = \sqrt{\langle A_n|A_n\rangle}$. If $b_n = 0$, exit the loop else continue.
 - (d) $|K_n\rangle = \frac{1}{b_n} |A_n\rangle$
 - (e) $a_n = \langle K_n|H|K_n\rangle$

This algorithm has numerical instabilities due to the round-off errors and it requires either a full or a partial re-orthogonalization to be carried out to ensure the orthogonality between Krylov vectors. This procedure is basically a Gram-Schmidt process applied to Krylov vectors/operators after every iteration. Above algorithm can also be used for operators [47] with redefining the inner products accordingly. Once the Lanczos coefficients are obtained using this algorithm, we can write the recursion relations and solve them.

To obtain the time evolution of these vectors, recursion relations in Eq. ??, 8 can be written in a vector-matrix linear ordinary differential equation form given in Eq. A1.

$$\frac{d\vec{\phi}}{dt} = M\vec{\phi} \quad (\text{A1})$$

where $\vec{\phi} = (\phi_0, \phi_1, \dots, \phi_{\mathbb{K}-1})^T$ and M is a tridiagonal matrix which has a different form for states M_s and operators M_o .

These matrices are used for obtaining state and operator complexities which are given by Eq. A2 and Eq. A3 respectively.

$$M_s = -i \begin{bmatrix} a_0 & b_1 & 0 & 0 & \dots \\ b_1 & a_1 & b_2 & 0 & \dots \\ 0 & b_2 & a_2 & b_3 & \dots \\ \vdots & \ddots & \ddots & \ddots & b_{\mathbb{K}-1} \\ 0 & 0 & \dots & b_{\mathbb{K}-1} & a_{\mathbb{K}-1} \end{bmatrix} \quad (\text{A2})$$

$$M_o = \begin{bmatrix} 0 & -b_1 & 0 & 0 & \dots \\ b_1 & 0 & -b_2 & 0 & \dots \\ 0 & b_2 & 0 & -b_3 & \dots \\ \vdots & \ddots & \ddots & \ddots & -b_{\mathbb{K}-1} \\ 0 & 0 & \dots & b_{\mathbb{K}-1} & 0 \end{bmatrix} \quad (\text{A3})$$

The solution to the differential equation in Eq. A1 can be given as $\vec{\phi}(t) = e^{Mt}\vec{\phi}(0)$ where $\vec{\phi}(0) = (1, 0, 0, \dots, 0)^T$ and is also expressed by the following recursion relation.

$$\dot{\phi}_n(t) = b_n\phi_{n-1}(t) - b_{n+1}\phi_{n+1}(t) \quad (\text{A4})$$

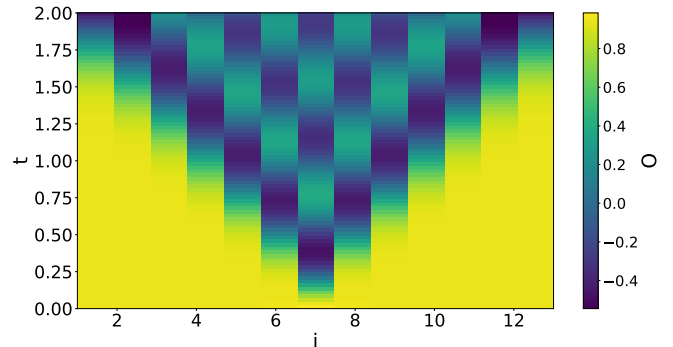


FIG. 6: Lightcone at $N = 13, J/h = 1.0, m = 0.05, \beta = 0.25, l_{\max} = 0.05$

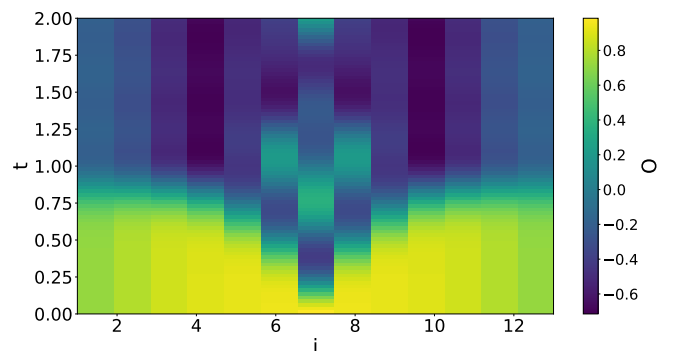


FIG. 7: Lightcone at $N = 13, J/h = 1.0, m = 0.05, \beta = 0.25, l_{\max} = 3.0$

A fourth-order Runge Kutta (RK4) method is then used to solve this recursion relation numerically.

Appendix B: Details on Thermal State Preparation

The purification procedure used to obtain the thermal states can be quickly summarized as follows.

We start with an infinite temperature Thermofield double state $|\text{TFD}(\infty)\rangle$ which can be initialized as

$$|\text{TFD}(\infty)\rangle = \mathbf{1}/\sqrt{2} \quad (\text{B1})$$

into a Matrix Product Operator (MPO) and evolved under imaginary time evolution with Time-Evolving Block Decimation (TEBD) techniques (using $e^{-\beta H}$, where H is the Hyperbolic Ising Hamiltonian).

If one continues the time evolution indefinitely this algorithm eventually reaches the ground state of the model. However, stopping at a desired β allows us to obtain the thermal states of the Hyperbolic Ising model in terms of an MPO.

With access to the thermal states of the model, we can calculate the OTOCs constructed using two local oper-

ators $W_i(t)$ and V_j where $W(t) = e^{iHt}W(0)e^{-iHt}$, combined into the double commutator.

$$C(t) = \langle ||[W_i(t), V_j]||^2 \rangle = 2(1 - \text{Re}[F_{ij}(t)]), \quad (\text{B2})$$

where $\langle . \rangle = \frac{1}{Z} \text{Tr}[e^{-\beta H} .]$ corresponds to the thermal expectation value at inverse temperature β and $F_{ij}(t)$ is known as the out-of-time-ordered correlator (OTOC). Other terms in the double commutator become irrelevant after a short time scale and hence can be omitted.

$$F_{ij}(t) = \langle W_i(t)^\dagger V_j(0)^\dagger W_i(t) V_j(0) \rangle. \quad (\text{B3})$$

In our calculations, we take $W(t) = \sigma^z(t)$, $V = \sigma^z$ and fix the position of the $W(t)$ operator at the center of the lattice chain which is the site $(N + 1)/2$. we then place the operator V at different lattice sites i and measure $F_{ij}(t)$

For constructing the lightcone we need to calculate the OTOC at all sites of the spin chain which leads to the following propagation patterns in Fig. 6, 7. As can be seen from these two plots, as the background curvature increases, the lightcone becomes warped. In [48] we showed in detail that depending on the curvature l_{max} and the nearest-neighbor coupling strength J it is possible to achieve different kinds of scrambling behavior ranging from linear to logarithmic using OTOCs calculated at infinite temperature.